# High-Frequency Surface Wave Radar Performance Analysis for CA-CFAR Algorithm in K-distributed Clutter

Diego da Silva de Medeiros, Rômulo Fernandes da Costa, Naiara Tieme Mippo, Dimas Irion Alves, and Renato Machado

***Abstract*— This paper analyzes the performance of a cell-averaging constant false alarm rate (CA-CFAR) algorithm designed for K-distributed clutter in High-Frequency Surface Wave Radar applications (HFSWR). Due to complex scattering mechanisms, the clutter returns in the range-Doppler spectrum are highly non-homogeneous. This study compares a closed-form probability of detection of the K-distribution CA-CFAR to a numerical simulation of sea clutter based on a physical sea radar cross-section (RCS) model, which considers wind conditions and operating parameters. The simulation shows that the closed-form analytical expression acts as an upper bound for detector performance, which is degraded in practice by the strong peaks of the clutter power.**

***Keywords*— HFSWR, radar simulation, performance analysis, K-distribution**

## I. INTRODUCTION

Ship detection in high-frequency surface wave radar (HFSWR) is affected by sea clutter, which has a strong and complex pattern and can mask ship echoes. Sea clutter is experienced as two strong lines in the radar image, with low power in far ranges but considerably stronger and spread in near ranges. Therefore, heavy-tailed distributions, such as Weibull [1] or K [2], are better candidates to represent sea clutter. Although both Weibull and K are compound Gaussian distributions, K-distribution is better suited to model sea clutter, as its parameters are more related to physical phenomena [3].

In this context, the cell averaging constant false alarm rate (CA-CFAR) is one of the most traditional detection techniques in the radar field, as it achieves a good target detection rate while maintaining false alarms at constant and acceptable levels [4]. Recently, the theoretical performance of the CA-CFAR, considering a K-distributed clutter scenario, was derived in terms of low computational cost closed-form expressions [5]. However, in HFSWR, as the sea clutter has a strong non-homogeneous statistical behavior, the classical CA-CFAR technique usually fails to guarantee the expected theoretical performance, as already seen in the Weibull-distributed clutter scenario [6].

In this paper, the performance of the HFSWR in an environment with K-distributed sea clutter is evaluated, considering a clutter model based on the physics of the sea, presented in [7], [8]. It is verified that, as the ideal homogenous condition is lost, the performance of the detector is severely degraded when confronted with theoretical performance. The spikier clutter is reflected as a decrease in the shape parameter of the K-distribution, a behavior corroborated by the obtained performance results.

The next section presents the clutter models used in this study, as well as the closed-form expressions used as reference results. Section III presents the analysis, focusing on three different regions of the HFSWR's range-Doppler map. Finally, Section IV concludes the discussion.

D. Medeiros, R. F. da Costa, N. T. Mippo, D. I. Alves, and R. Machado are with the Department of Telecommunications, Aeronautics Institute of Technology, 12228-900, São José dos Campos, SP, Brazil, e-mails: {medeiros, rfcosta, naiara, dimasirion, machado}@ita.br.

## II. DEVELOPMENT

### A. Simulation of sea clutter model

The HFSW radar output is an image with the received information, oriented horizontally in the Doppler dimension and vertically in the Range dimension. This range-Doppler map contains signal returns from targets present in the area and signals from sea clutter returns. As radar waves encounter resonance with oncoming and outgoing sea waves, the clutter signal is characterized mainly by two main peaks in the Doppler dimension that extend across almost all the Range dimension. These two peaks are also known by the term Bragg lines [3].

To obtain the power $P_r$ of clutter echoes for each pixel in a range-Doppler power spectrum image, the radar equation can be used, defined as

$$P_r(R, \omega_D) = \frac{P_t G_t G_r \lambda^2 F_p^4(R)}{(4\pi)^3 R^4} \sigma_C(\omega_D), \tag{1}$$

where $P_t$ is the transmitted power, $G_t$ and $G_r$ are transmitter and receiver gains respectively, $\lambda$ is the radar wavelength, $F_p(R)$ is an attenuation factor for propagation losses, and $\sigma_C(\omega_D)$ is the effective radar cross-section (RCS) of the sea clutter.

Grosdidier, Baussard, and Khenchaf [9] recommended that the attenuation factor $F_p$ can be obtained from computational models such as GRWAVE [10]. Propagation losses in HFSWR increase drastically with higher frequencies, eventually reducing surface echoes below background noise.

The sea clutter model adopted in this paper is based on [7], [8], [11], [9]. In these works, the sea clutter radar cross-section (RCS) is modeled by two components. The first-

order component models the two Bragg lines, with the large-scale resonance between radar and sea waves. The small-scale clutter variation is modeled by the second-order component, representing the double backscattering phenomena. The two components are summed to obtain the clutter RCS, normalized for scattering area and angular frequency; thus, its units are $\frac{\mathrm{m^2/m^2}}{\mathrm{rad/s}}$ [7]. Then

$$\sigma_C(\omega_D) = \sigma_{C1}(\omega_D) + \sigma_{C2}(\omega_D), \tag{2}$$

where $\omega_D$ is Doppler angular frequency, $\sigma_{C1}(\omega_D)$ is the first-order normalized RCS, and $\sigma_{C2}(\omega_D)$ is the second-order normalized RCS. The normalized first-order RCS is the result of a resonance effect between the radar wave and sea waves of approximately half the wavelength of the radar wave, and is written as [8]

$$\sigma_{C1}(\omega_D) = 16\pi k_0^2 \Delta\rho_s \sum_{m=\pm1} S(m\vec{K}) \frac{K^{2.5}\cos(\phi_0)}{\sqrt{g}} \times \mathrm{Sa}^2\left[\frac{\Delta\rho_s}{2}\left(\frac{K}{\cos(\phi_0)} - 2k_0\right)\right], \tag{3}$$

where $k_0$ is the wavenumber of the radar wave, $\Delta\rho_s$ is the pulse spacial length (or patch width), $S(m\vec{K})$ is the sea directional spectrum, $\vec{K}$ is the wave vector of the sea wave, which is collinear to the incident radar wave, $\phi_0$ is a value representative of the bistatic angle, $g$ is gravitational acceleration, $\mathrm{Sa}(x) = \frac{\sin(x)}{x}$ is the unnormalized sinc function, also called sample function, and $K$ is the sea wave wavenumber, related to $\omega_D$ by

$$\omega_D = -m\sqrt{gK}, \tag{4}$$

$m$ being the summation index in $\sigma_{C1}$.

For a monostatic system, $\phi_0 = 0$, and so the RCS peaks are located at the Doppler frequency $f_B$ given by [12]

$$f_B = \pm\sqrt{\frac{gf_c}{\pi c}}, \tag{5}$$

where $f_c$ is the center frequency of the radar and $c$ is the speed of light constant.

The second-order sea RCS $\sigma_{C2}$ considers two waves of wavenumber $K_1$ and $K_2$, with $\vec{K_1} + \vec{K_2} = \vec{K}$ and is written as [11]

$$\sigma_{C2}(\omega_D) = 8\pi k_0^2 \Delta\rho_s \times \sum_{m_1=\pm1}\sum_{m_2=\pm1} \int_0^\infty \int_{-\pi}^{\pi} \int_0^\infty S(m_1\vec{K_1}) S(m_2\vec{K_2}) \times \delta\left(\omega_D + m_1\sqrt{gK_1} + m_2\sqrt{gK_2}\right)\cos(\phi_0)|\Gamma|^2 K^2 \times \mathrm{Sa}^2\left[\frac{\Delta\rho_s}{2}\left(\frac{K}{\cos(\phi_0)} - 2k_0\right)\right] K_1 dK_1 d\theta_1 dK, \tag{6}$$

where $\vec{K_1}$ and $\vec{K_2}$ are respectively the corresponding wave vectors of the two considered waves, $\theta_1$ is the direction angle of $K_1$, $\delta$ is the Dirac delta function, and $\Gamma = \Gamma_H + \Gamma_E$ is a coupling coefficient considering a hydrodynamic term $\Gamma_H$ and an electromagnetic term $\Gamma_E$. From [11], [8], $\Gamma_H$ is

$$\Gamma_H = \frac{1}{2}\left[K_1 + K_2 + \frac{g}{\omega_1\omega_2}(K_1K_2 - \vec{K_1}\vec{K_2}) \times \frac{gK + (\omega_1+\omega_2)^2}{gK - (\omega_1+\omega_2)^2}\right], \tag{7}$$

where $\omega_1$ and $\omega_2$ are the angular frequencies of the sea waves, and $\Gamma_E$ is

$$\Gamma_E = \frac{-(\vec{K_1}\hat{\rho_2})[\vec{K_2}(\vec{K_1} - k_0\hat{\rho_2})]}{K\cos(\phi_0)\sqrt{\vec{K_1}(\vec{K_1} - 2k_0\hat{\rho_2})}}, \tag{8}$$

where $\rho_2$ is a normalized vector pointing from the second scattering point to the receiver. For monostatic systems, the models can be simplified by considering $\phi_0 = 0$ and $\hat{\rho_2} = \hat{K} = \vec{K}/K$. The detailed presentation of the RCS model is out of the scope of this work, but the interested reader is referred to [11].

An important component of (3) and (6) is the sea spectrum $S(\vec{k})$, which acts as a measurement of sea state conditions taking into account environmental factors such as wind speed and direction. The sea spectrum model used in [11] modifies the Pierson-Moskowiz model [13] by including a cardioid directional distribution and can be defined as

$$S(m\vec{K}) = \left[\frac{0.0081}{4K^2}\exp\left(\frac{-0.74g^2}{K^2U_w^4}\right)\right] \times \left[\frac{4}{3\pi}\cos^4\left(\frac{\theta_{\vec{K}} + \frac{(1-m)\pi}{2} - \theta_w}{2}\right)\right], \tag{9}$$

where $U_w$ and $\theta_w$ are the wind speed and direction angle, respectively, and $\theta_{\vec{K}}$ is the direction angle of wave vector $\vec{K}$.

It is important to highlight that (1) is a deterministic equation for sea clutter power. Power per pixel is made to fluctuate according to a desired distribution by multiplying $P_r$ by a random variable. Figure 1 shows the sea clutter contributions caused by $\sigma_{C1}(\omega_D)$ and $\sigma_{C2}(\omega_D)$ that form the overall sea clutter, based on parameters shown in Table I.

### *B. CA-CFAR detection for K-distributed clutter*

In the detection stage, the Probability of Detection $P_d$ and the Probability of False Alarm $P_{fa}$ are two important metrics to evaluate radar performance. In this context, the CA-CFAR is one of the most traditional detection techniques, because it maximizes $P_d$ while maintaining $P_{fa}$ at a constant acceptable level [4].

The model in [5] considers a Swerling II (exponentially distributed) target and a K-distributed clutter with fully correlated texture in a square-law detector. The received complex baseband signals follow a binary hypothesis test

$$\mathcal{B}_{\mathcal{H}_0} = \xi X + j\xi Y \tag{10}$$

$$\mathcal{B}_{\mathcal{H}_1} = (\xi X + A) + j(\xi Y + B), \tag{11}$$

where $\mathcal{H}_0$ and $\mathcal{H}_1$ denote respectively the clutter-only and the clutter-plus-target cases, $X, Y \sim \mathcal{N}(0, 1/2)$ (Normal-distributed, with mean 0 and variance 1/2), $\xi \sim \mathcal{NK}\left(\nu, 2\sigma_c^2\right)$ (Nakagami-distributed, with shape $\nu$ and spread $2\sigma_c^2$), and $A, B \sim \mathcal{N}\left(0, \sigma_t^2\right)$ (Normal-distributed, with mean 0 and variance $\sigma_t^2$). To the power level, the signals are written as

$$Z_{\mathcal{H}_0} = |\mathcal{B}_{\mathcal{H}_0}|^2 = T\,S \tag{12}$$

$$Z_{\mathcal{H}_1} = |\mathcal{B}_{\mathcal{H}_1}|^2 = U^2 + V^2, \tag{13}$$

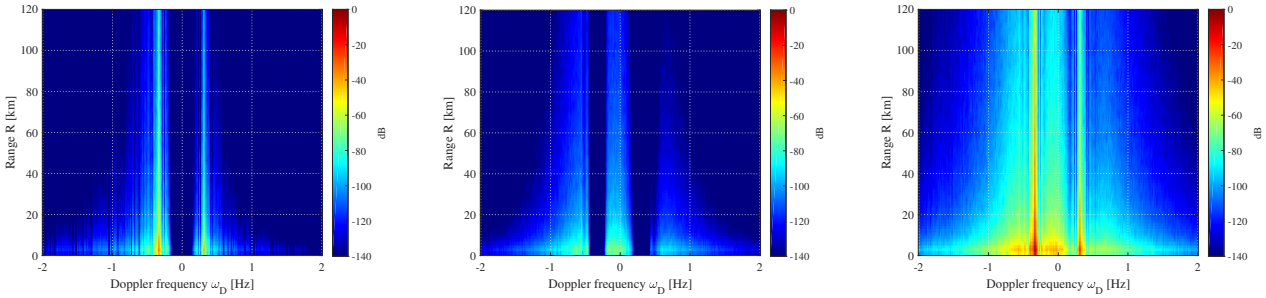


(a) (b) (c)

Fig. 1

NORMALIZED RANGE-DOPPLER POWER SPECTRUM IN DB OF THE FIRST-ORDER (A) AND SECOND-ORDER (B) COMPONENTS OF THE SEA CLUTTER AND THE FULL POWER SPECTRUM OF THE SIMULATED SEA CLUTTER (C), FOR PARAMETERS IN TABLE I.

where $T \triangleq \xi^2 \sim \mathcal{G}\left(\nu, \frac{2\sigma_c^2}{\nu}\right)$ and $S \triangleq \left(X^2 + Y^2\right) \sim \mathcal{E}(1)$ represent the *texture* and *speckle* components of the K-distributed clutter, respectively, $U \triangleq (\xi X + A)$, and $V \triangleq (\xi Y + B)$.

In this scenario, the signal-to-clutter ratio (SCR) is

$$\text{SCR} \triangleq \frac{\mathbb{E}\left\{|A + jB|^2\right\}}{\mathbb{E}\left\{|\xi X + j\xi Y|^2\right\}} = \frac{\sigma_t^2}{\sigma_c^2}. \tag{14}$$

The threshold used by the CA-CFAR is $T = \hat{\gamma}\tau$, where $\hat{\gamma}$ is an estimate of the clutter power, the average of the $N$ the reference cells, and $\tau$ is an adjusting constant, used to set the $P_{fa}$ to an acceptable level.

The metrics $P_{fa}$ and $P_d$ can then be found in [4] and are given by

$$P_{fa} = \int_0^\infty \int_{\hat{\gamma}\tau}^\infty f_Z(z|\mathcal{H}_0)\,\mathrm{d}z \;\; f_{\hat{\gamma}}(\hat{\gamma})\,\mathrm{d}\hat{\gamma} \tag{15}$$

$$P_d = \int_0^\infty \int_{\hat{\gamma}\tau}^\infty f_Z(z|\mathcal{H}_1)\,\mathrm{d}z \;\; f_{\hat{\gamma}}(\hat{\gamma})\,\mathrm{d}\hat{\gamma} \tag{16}$$

where $f_Z(z|\mathcal{H}_0)$ and $f_Z(z|\mathcal{H}_1)$ are respectively the probability density function (PDF) of $Z$ under hypotheses $\mathcal{H}_0$ and $\mathcal{H}_1$, and $f_{\hat{\gamma}}(\hat{\gamma})$ is the PDF of the $\gamma$ estimate.

Medeiros [5] has worked with (15) and (16), and the following closed-form expression for $P_{fa}$ was obtained

$$P_{fa} = \left(\frac{\tau}{N}\right)^\nu \frac{\Gamma(2\nu)\Gamma(\nu+N)}{\Gamma(\nu)\Gamma(2\nu+N)} \times {}_2F_1\left(2\nu, \nu+N, 2\nu+N, 1-\frac{\tau}{N}\right), \tag{17}$$

where ${}_2F_1(a,b,c,z)$ is the Gauss hypergeometric function; and the following closed-form expression for $P_d$

$$P_d = 1 - \frac{1}{\Gamma(N)\Gamma(\nu)^2}\left(\frac{\tau}{N\nu\text{SCR}}\right) \times \mathbf{H}\left[\mathbf{z}_\text{D}; (\delta_\text{D}, \mathbf{D}_\text{D}); (\beta_\text{D}, \mathbf{B}_\text{D}); \mathcal{L}_\text{D}\right], \tag{18}$$

where $\mathbf{H}[\cdot]$ is the Fox H-function [14], in which $\delta_\text{D} = \begin{bmatrix}0 & \nu+1 & N+1 & 0 & \nu & 1\end{bmatrix}$, $\beta_\text{D} = 2$, $\mathbf{B}_\text{D} = \begin{bmatrix}-1 & 0\end{bmatrix}$, $\mathcal{L}_\text{D}$ is a suitable contour on the complex plane provided $0 < \text{Re}\{s_1\} < 1 - \text{Re}\{s_2\}$ and $0 < \text{Re}\{s_2\} < \min(\nu, 1 - \text{Re}\{s_1\})$, $\mathbf{z}_\text{D} = \begin{bmatrix}\frac{\tau}{N\nu\text{SCR}} & \frac{1}{\nu\text{SCR}}\end{bmatrix}$, and

$$\mathbf{D}_\text{D} = \begin{bmatrix}1 & -1 & -1 & 0 & 0 & -1\\ 0 & 0 & 0 & 1 & -1 & -1\end{bmatrix}^T$$

The expressions (17) and (18) are faster to be calculated by computers than the previously available equations. This paper considers these expressions as a reference to the performance analysis.

TABLE I
CLUTTER SIMULATION PARAMETERS.

| Parameter | Value | Unit |
|---|---|---|
| Transmission power $P_t$ | 16 | kW |
| Transmission gain $G_t$ | 10 | - |
| Receiver gain $G_r$ | 100 | - |
| Attenuation factor $F_p(R)$ | 1 | - |
| Center frequency $f_c$ | 10 | MHz |
| Bandwidth $B_w$ | 100 | kHz |
| Wind speed $U_w$ | 5 | m/s |
| Wind direction angle $\theta_w$ | 45 | deg |
| Radar angle $\theta_r$ | 90 | deg |

## III. RESULTS

Table I presents the parameters used to simulate clutter samples in the HFSWR using the sea clutter model described in Section II-A. The parameter values were selected to reflect real situations, which are traditionally used in literature. The attenuation factor for propagation losses value $F_p$ was set to unity for simplicity since the objective of this work is to evaluate the performance of CA-CFAR under K-distributed clutter. No background noise was applied to the simulator.

A 7x7 CFAR window is used to estimate the threshold value, and the probability of detection $P_d$ is measured through Monte Carlo simulations. We consider three regions of clutter in the analysis, as shown in Fig. 2.(a), considering different levels of clutter influence and homogeneity. The weakest and

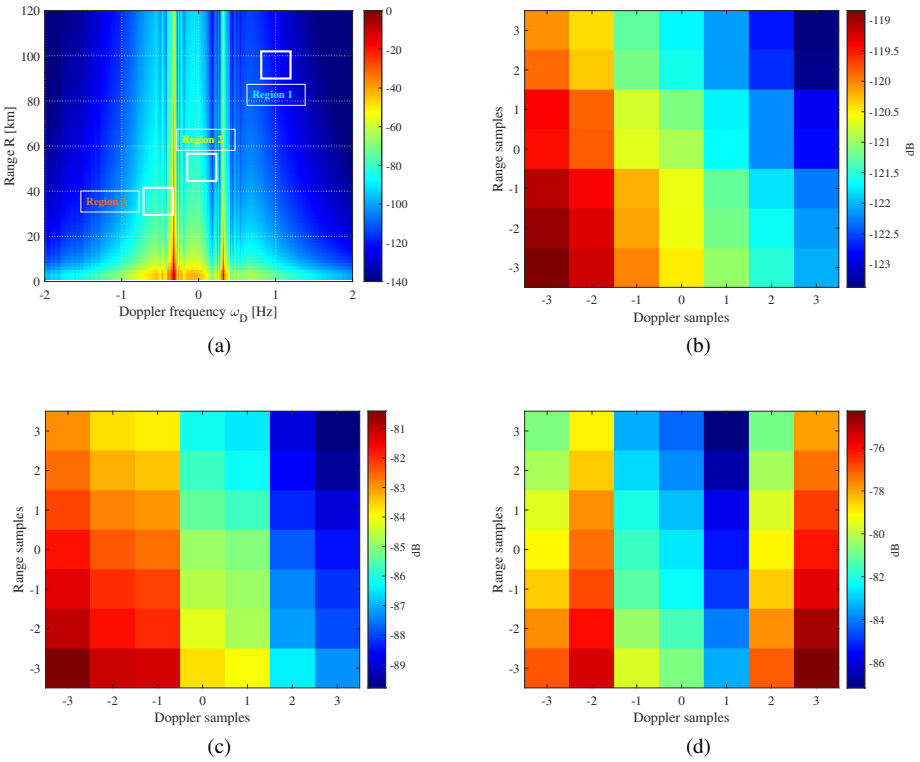


Fig. 2

AVERAGE OF THE 1024 SAMPLES OF THE SEA CLUTTER RANGE-DOPPLER POWER SPECTRUM IN DB USED IN SIMULATION, AND THE REGIONS OF ANALYSIS. (A) FULL RANGE-DOPPLER POWER SPECTRUM; (B) REGION 1; (C) REGION 2; (D) REGION 3.

more homogeneous clutter influence is in Region 1, located at a Doppler frequency of 1.00 Hz and 96 km from the radar. A more moderate clutter influence is seen in Region 2, located at a Doppler frequency of 0.04 Hz and 51 km away from the radar. For the strongest clutter influence and lowest homogeneity, Region 3 is at a Doppler frequency of -0.51 Hz and 36 km away from the radar, approaching the clutter peak. 1024 simulated windows are generated for measuring Pd at each region.

Considering that the closed-form expressions in [5] are obtained based on a homogeneous clutter scenario, a variation in results is expected, as the homogeneous condition is lost. As the nature of the clutter RCS model used in this work comprises several peaks spread across Doppler, the $P_d$ measured with a threshold estimated from a CFAR window near clutter peaks will be decreased. If the clutter peak contaminates the CUT, the measured $P_d$ will be falsely increased, as it represents the condition of the constant false alarm being broken by false positives.

The differences in clutter pattern can also be seen in Figure 2 by examining the range of amplitudes of the three highlighted regions. The samples of Regions 1, 2, and 3 present a range of fluctuation of about 4 dB, 8 dB, and 10 dB respectively. The average clutter strength of Region 1 is also weaker than Regions 2 and 3, where the former is located around -120 dB, while the latter two are around -85 dB and -80 dB.

### A. *Comparison of the closed form with simulation results*

Figures 3, 4, and 5 show the measured $P_d$ as a function of the $P_{fa}$ for all three regions, for three different values of $P_{fa}$. The impact of the loss of the homogeneity condition can be seen by the comparison with the theoretical result, obtained with the closed-form expressions 17 and 18. As an example, for $\nu = 3.5$ and $P_{fa} = 10^{-4}$, the green curve of Figures 3, 4, and 5 shows that the mismatch of the theoretical to the simulated $P_d$ (distance from the solid to the dashed curves) is about 0.11, 0.36 and 1.69, respectively to Regions 1, 2 and 3. Furthermore, from Figure 5, it can be seen that the spikiness of the sea clutter is reflected as a decrease in the K-distribution shape parameter, as performances for the simulated scenario for $\nu = 2.5$ and theoretical scenario for $\nu = 1.8$ are similar.

The results show that the loss in the homogenous condition of the clutter degrades the performance of the detector. The theoretical closed-form expressions, in this sense, act as a performance upper bound, as it considers that the conditions of the sea clutter are ideally homogeneous.

## IV. CONCLUSIONS

This work conducted a performance analysis for an HFSWR operating in a scenario with K-distributed clutter and exponentially distributed target echo signals. Deterministic models that account for physical factors to generate reliable clutter samples were used as a basis for the simulation. The simulation results

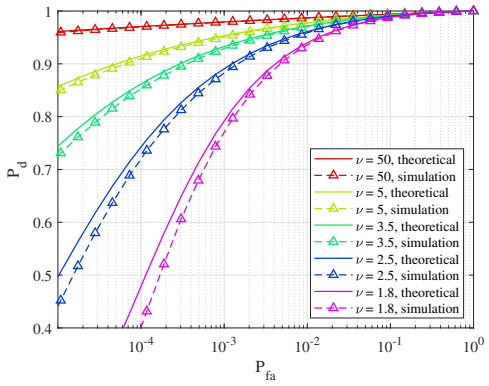


Fig. 3
PROBABILITY OF DETECTION, FOR REGION 1, FOR $N = 40, \sigma_c = 0.05$ AND $\sigma_t = 1$.

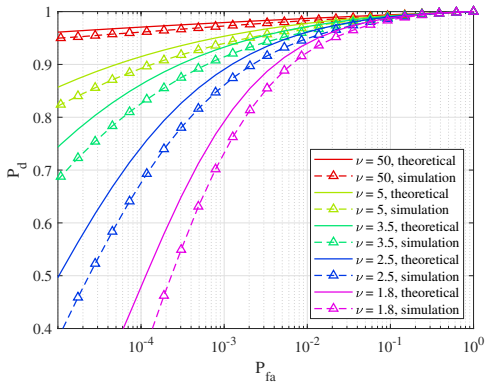


Fig. 4
PROBABILITY OF DETECTION, FOR REGION 2, FOR $N = 40, \sigma_c = 0.05$ AND $\sigma_t = 1$.

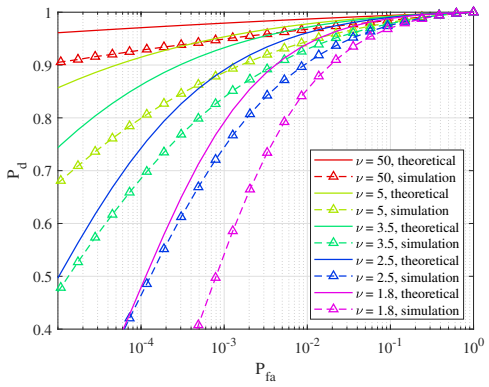


Fig. 5
PROBABILITY OF DETECTION, FOR REGION 3, FOR $N = 40, \sigma_c = 0.05$ AND $\sigma_t = 1$.

were then compared to theoretical closed-form expressions in the literature. Results show that the performance of the HFSWR is degraded by strong peaks caused by the first and second-order components of the clutter RCS, which violate the homogeneity condition of the cell averaging constant false alarm rate (CA-CFAR) detector. The theoretical closed-form expressions represented an upper bound for the performance achievable by HFSWR in regions weakly affected by clutter returns. These results suggest that future detection algorithms for HFSWR need to consider the strongly non-homogeneous behavior of the sea clutter, which is far from the conditions expected in traditional detection algorithms.

## ACKNOWLEDGEMENTS

This work was supported in part by IACIT Technology Solutions, by the São Paulo Research Foundation (FAPESP) under Grants 2020/09838-0 and 2021/03923-9, and the Brazilian National Council for Scientific and Technological Development (CNPq).

## REFERENCES

[1] X. Wang, Y. Li, N. Zhang, and Y. Cong, "An Automatic Target Detection Method Based on Multidirection Dictionary Learning for HFSWR," *IEEE Geosci. Remote Sens. Lett.*, pp. 1–5, 2021.

[2] A. Cheeseman, "Adaptive Waveform Design and CFAR Processing for High Frequency Surface Wave Radar," M.S. Thesis, University of Toronto, Toronto, Nov. 2017. [Online]. Available: https://tspace.library.utoronto.ca/handle/1807/79106

[3] G. A. Fabrizio, *High Frequency Over-the-Horizon Radar: Fundamental Principles, Signal Processing, and Practical Applications*, 1st ed. McGraw-Hill Education, 2013.

[4] M. A. Richards, J. A. Scheer, and W. A. Holm, Eds., *Principles of Modern Radar: Basic Principles*. SciTech Publishing, 2010.

[5] D. S. Medeiros, F. D. A. García, R. Machado, J. C. S. S. Filho, and O. Saotome, "CA-CFAR Performance in K-Distributed Sea Clutter With Fully Correlated Texture," *IEEE Geosci. Remote Sens. Lett.*, vol. 20, pp. 1–5, 2023.

[6] D. S. Medeiros, R. F. Costa, D. I. Alves, R. Machado, and O. Saotome, "High-frequency surface wave radar performance analysis for CA-CFAR algorithm in Weibull-distributed clutter," in *Remote Sensing of the Ocean, Sea Ice, Coastal Waters, and Large Water Regions 2022*, vol. 12263. SPIE, Oct. 2022.

[7] E. Gill and J. Walsh, "High-frequency bistatic cross sections of the ocean surface," *Radio Science*, vol. 36, no. 6, pp. 1459–1475, 2001.

[8] E. Gill, W. Huang, and J. Walsh, "On the development of a second-order bistatic radar cross section of the ocean surface: A high-frequency result for a finite scattering patch," *IEEE J. Ocean. Eng.*, vol. 31, no. 4, pp. 740–750, 2006.

[9] S. Grosdidier, A. Baussard, and A. Khenchaf, "HFSW radar model: Simulation and measurement," *IEEE Trans. Geosci. Remote Sens.*, vol. 48, no. 9, pp. 3539–3549, 2010.

[10] M. Whitington and R. Thomas, "Software for prediction and analysis of ground wave propagation loss," SURVEILLANCE RESEARCH LAB SALISBURY (AUSTRALIA), Tech. Rep., 1992.

[11] E. W. Gill, "The scattering of high frequency electromagnetic radiation from the ocean surface: An analysis based on a bistatic ground wave radar configuration," Ph.D. dissertation, Memorial University of Newfoundland, 1999.

[12] T. Ponsford and J. Wang, "A review of high frequency surface wave radar for detection and tracking of ships," *Turkish Journal of Electrical Engineering and Computer Sciences*, vol. 18, no. 3, pp. 409–428, 2010.

[13] W. J. Pierson Jr and L. Moskowitz, "A proposed spectral form for fully developed wind seas based on the similarity theory of sa kitaigorodskii," *Journal of geophysical research*, vol. 69, no. 24, pp. 5181–5190, 1964.

[14] A. M. Mathai, R. K. Saxena, and H. J. Haubold, *The H-Function: Theory and Applications*. Springer-Verlag, 2010.